

Supplementary Information for
Electronic and Vibrational Surface-enhanced Raman Scattering:
from Atomically Defined Au(111) and (100) to Roughened Au

*Motoharu Inagaki,^{a†} Taichi Isogai,^a Kenta Motobayashi,^a Kaiqiang Lin,^b Bin Ren,^c and
Katsuyoshi Ikeda^{*,a,d}*

^a Department of Physical Science and Engineering, Nagoya Institute of Technology, Gokiso,
Showa, Nagoya 466-8555, Japan.

^b Institut für Experimentelle und Angewandte Physik, Universität Regensburg, Germany

^c State Key Laboratory of Physical Chemistry of Solid Surfaces, Department of Chemistry, Xiamen
University, China

^d Frontier Research Institute for Materials Science (FRIMS), Nagoya Institute of Technology,
Gokiso, Showa, Nagoya 466-8555, Japan.

Corresponding Author

*kikeda@nitech.ac.jp.

†Present address: Asahi Intecc Co. Ltd. Akatsuki-cho, Seto, Aichi 489-0071, Japan.

1. ERS vs. PL

There are two predominant mechanisms for SERS background generation: ERS and PL. Both of them are recognized as plasmon-enhanced intraband transitions of electrons in the *sp*-conduction band of a metal. To distinguish them, the ratio of intensities between the anti-Stokes and the Stokes can be a reliable indication as follows. According to Ref. (24), the power spectrum for ERS in the absolute wavenumber plotting ($\tilde{\nu} = \nu/c$ in cm^{-1} , where c is the velocity of light) can be expressed by:

$$I_{\text{ERS}}(\tilde{\nu}) \propto [1 + n(\tilde{\nu}_i - \tilde{\nu})], \quad (\text{S1})$$

where $\tilde{\nu}_i$ and $\tilde{\nu}$ are incident and scattered photon energies in cm^{-1} . n is the Bose-Einstein thermal factor. In the relative wavenumber plotting ($\tilde{\nu}^\Delta = \tilde{\nu}_i - \tilde{\nu}$) of Raman spectra, therefore, Eq. (S1) can be decomposed into two equations: $I_{\text{ERS}}(\tilde{\nu}_{\text{as}}^\Delta) \propto [n(\tilde{\nu}_m)]$ for the anti-Stokes and $I_{\text{ERS}}(\tilde{\nu}_s^\Delta) \propto [n(\tilde{\nu}_m + 1)]$ for the Stokes, where $\tilde{\nu}_{\text{as}}^\Delta \equiv -\tilde{\nu}_m = \tilde{\nu}_i - \tilde{\nu} < 0$ and $\tilde{\nu}_s^\Delta \equiv \tilde{\nu}_m = \tilde{\nu}_i - \tilde{\nu} > 0$, as shown in Eqs. (2) and (3). Therefore, one can expect that the anti-Stokes and Stokes branches must have a correlation expressed by: anti-Stokes/Stokes = $[n(\tilde{\nu}_m)]/[n(\tilde{\nu}_m + 1)] = \exp\left(\frac{-hc\tilde{\nu}_m}{k_B T}\right)$. On the other hand, the power spectrum for intraband PL in the absolute wavenumber plotting can be expressed by:

$$I_{\text{PL}}(\tilde{\nu}) \propto \tilde{\nu}[n(\tilde{\nu})]. \quad (\text{S2})$$

Eq. (S2) does not include $\tilde{\nu}_i$ as a parameter in the thermal factor, and hence, one cannot expect any correlations between anti-Stokes and Stokes branches in the relative wavenumber plotting. Therefore, if normal Raman signals measured at a flat metal surface originate from ERS, one can find the symmetry between the anti-Stokes and the Stokes branches after removal of the thermal

factor in Eq. (S1). In the case of SERS, the Purcell factor has to be deduced in addition to the thermal factor to evaluate the symmetry.

ERS in the conduction band of a metal must conserve the momentum difference between the initial and final electronic states. The transfer momentum from incident photons, q , has the order of δ^{-1} , where δ is the penetration depth at metal surface.⁵⁹ Thus, ERS spectra are dependent on the excitation energy even under off-resonant conditions. The spectral maximum of χ_{ERS}'' is known to be found at $\omega = qv_F$, where v_F is the Fermi velocity.^{58,59} Figure S1(a) shows the wavelength dependence of the penetration depth at Au(111), which was calculated using the optical constants of Au(111). The increase of the penetration depth at around 500 nm is caused by the contribution of *sp-d* interband transition of Au. Figure S1(b) shows the normalized spectra for χ_{ERS}'' of Au(111) obtained using different excitation wavelengths indicated by arrows in Fig. S1(a). The spectral maximum is clearly shifted to lower wavenumber with increasing the excitation energy, which agrees with the expected tendency from the decrease of the transfer momentum. This is also an evidence to support the observed signal originates from ERS. (The spectrum maximum for the 633-nm excitation is slightly different between Fig. S1(b) and Fig. 3(d). This is because these are measured with objectives with different NA, which affects to the magnitude of the transfer momentum.)

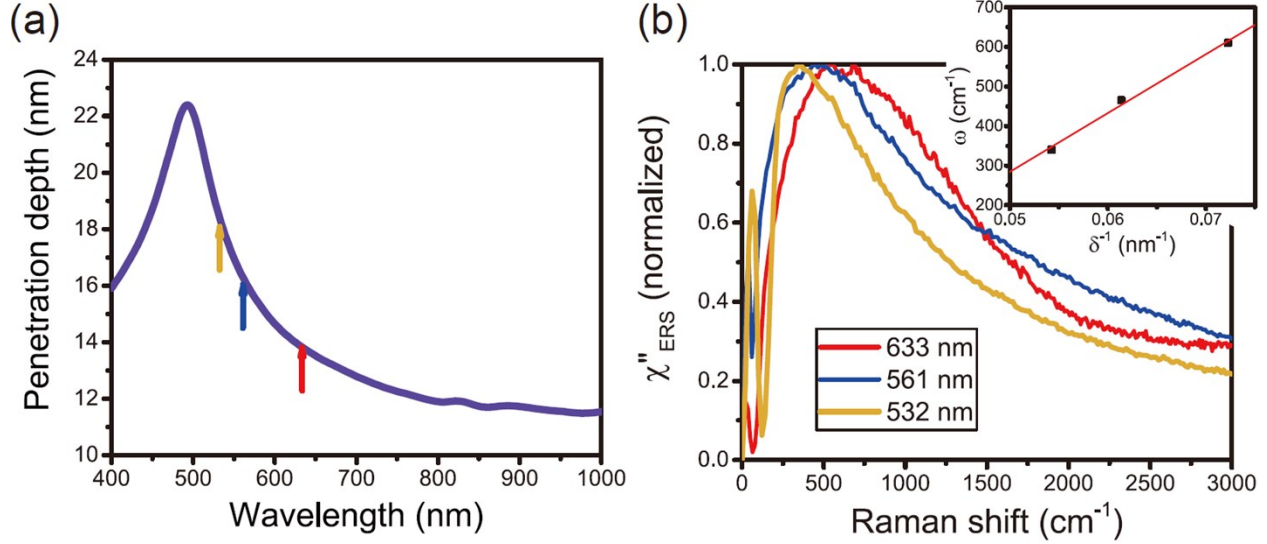


Figure S1. (a) Wavelength dependence of penetration depth at Au(111). (b) Normalized χ''_{ERS} spectra for Au(111) obtained using three different excitation wavelengths. Raw ERS spectra were measured using the same objective ($50\times$, $0.75NA$). Inset: the spectra maximum (ω) vs. the inverse of the penetration depth (δ^{-1}).

2. SERS spectra on single crystalline Au surfaces

Figure S2 shows SERS spectra for AuNP/MBT/Au(100) obtained using different size AuNPs. As shown in the log-scale plot, the anti-Stokes background signals seem to decay exponentially. Thus, the anti-Stokes background profiles have been often fitted with the Boltzmann function; the apparent local temperatures are estimated to be $T = 346$ K for ϕ 20 nm, 315 K for ϕ 40 nm, and 304 K for ϕ 60 nm by the Boltzmann fitting. However, these temperature values are overestimated because of the spectral profile of χ''_{ERS} for Au (see Fig. 3). Moreover, the apparent local temperature increases with decreasing the size of AuNP. This is related to the difference of the plasmon resonances in these samples (see Fig. 5).

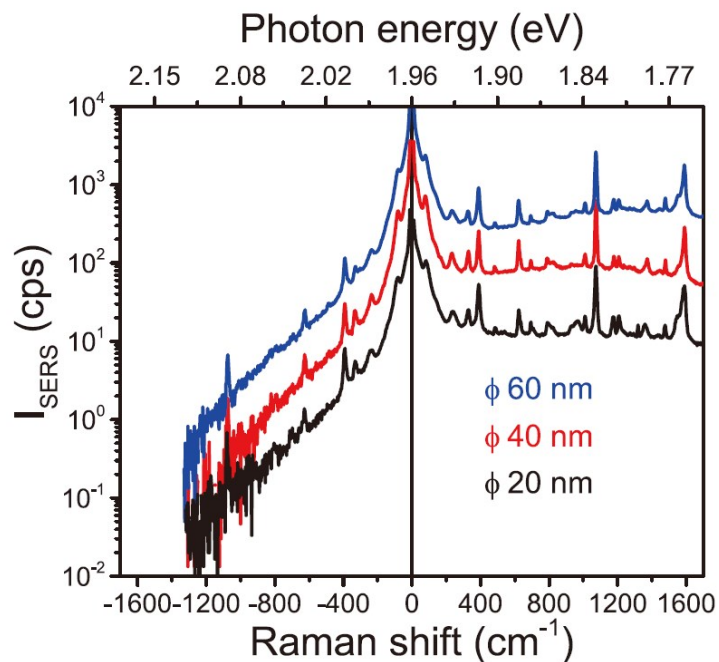


Figure S2. Raw gap-mode SERS spectra for AuNP(ϕ 20 nm)/MBT/Au(100), AuNP(ϕ 40 nm)/MBT/Au(100), and AuNP(ϕ 60 nm)/MBT/Au(100), measured with an objective (40 \times , 0.6NA).

The contribution of the plasmon resonances to SERS spectra is more clearly shown in Fig. S3. When SERS spectra shown in Fig. S2 are divided by the normal Raman spectra for MBT/Au(100), the thermal factor and the scattering efficiency factor are deduced from the spectra; note that the Purcell factor remains in this calculation. For both VSERS peaks and ESERS background, their relative intensities correlate with the plasmon resonance spectra.

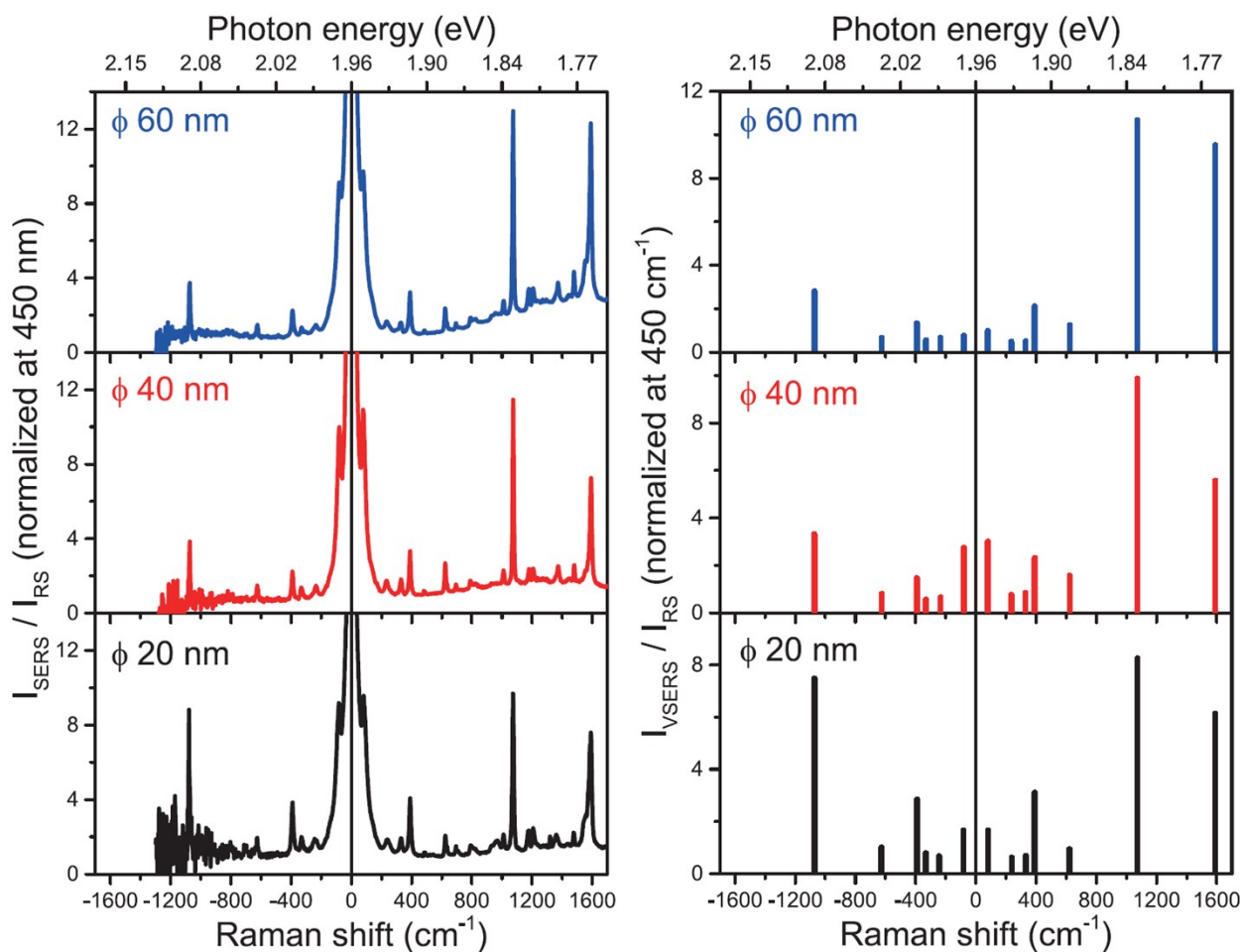


Figure S3. Left panel: SERS spectra of Fig. S1 are divided by RS spectra for MBT/Au(100) and normalized by ERS intensity at 450 cm^{-1} . These $I_{\text{SERS}}/I_{\text{RS}}$ spectra are overlaid in Fig. 5(c). Right panel: Normalized vibrational peak intensity plots ($I_{\text{VSERS}}/I_{\text{RS}}$) extracted from the left panel figure.

A measured SERS spectrum involves electronic and vibrational scattering susceptibilities modified by the Purcell factor, the Bose-Einstein thermal factor and the scattering efficiency factor. The thermal and scattering efficiency factors can be easily reduced from the measured spectrum. In Fig. S4, the raw SERS spectrum of (a) is converted to (b) using $T = 300$ K. One can see that the intense background feature in the low Raman-shift region of the raw spectrum is mainly

due to the thermal factor. Thus, VSERS features in this region are well revealed by this reduction. On the other hand, the Stokes and anti-Stokes branches are rather asymmetric because of the contribution of the Purcell factor. To reduce this contribution, the deduced spectrum of (b) is further divided by the EF_{ESERS} spectrum, which can be obtained as the background profile of $I_{\text{SERS}}(\text{AuNP/MBT/Au})/I_{\text{RS}}(\text{MBT/Au})$, as explained in the main text. The obtained χ_{SERS}'' spectrum is shown in Fig. S4(c); the Stokes and anti-Stokes features become nearly symmetric, indicating that χ_{SERS}'' is properly extracted from the raw spectrum. The background profile of the χ_{SERS}'' spectrum is similar to the χ_{RS}'' spectrum for MBT/Au, in which the anti-Stokes branch is created using the Stokes branch of χ_{RS}'' . From the comparison of the χ_{SERS}'' and χ_{RS}'' spectra, it is noticed that the ERS intensities in the low Raman-shift region are larger than the values expected from local field enhancement. This is presumably explained by the extra enhancement induced by the momentum transfer from plasmonic nanostructures.

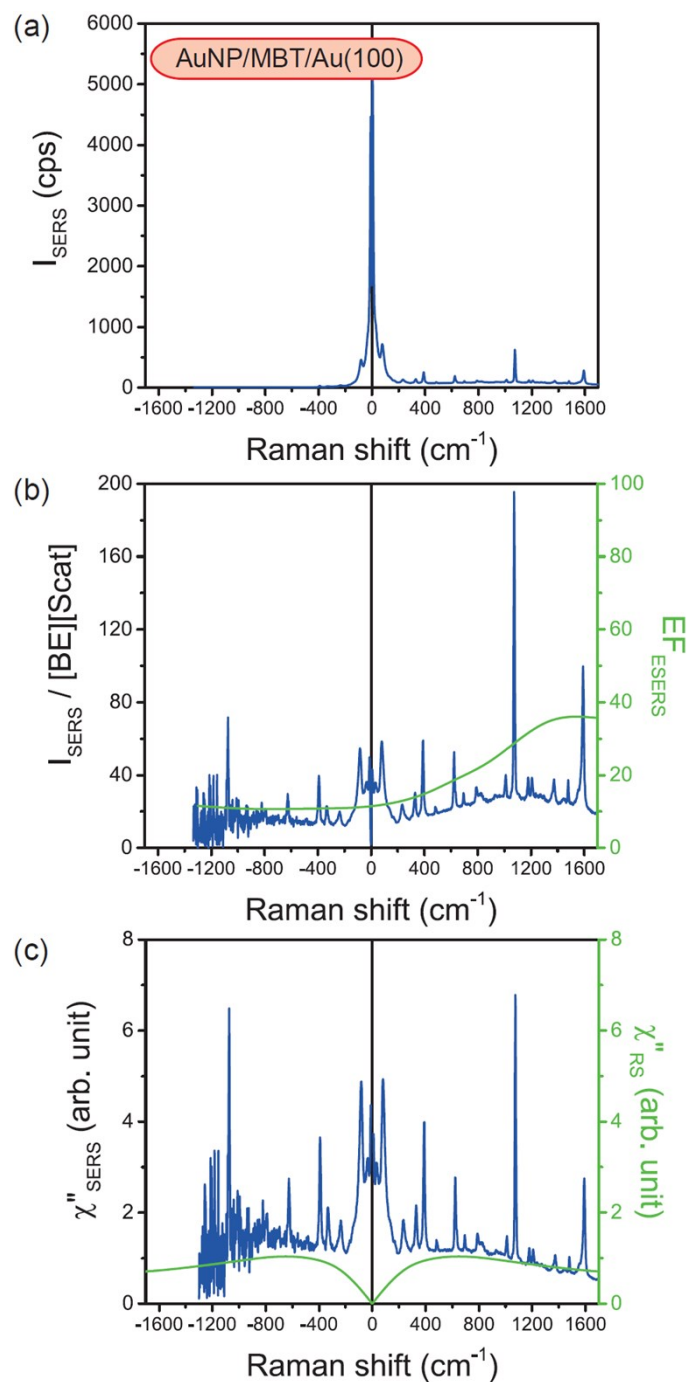


Figure S4. (a) Raw SERS spectrum measured for AuNP(ϕ 40 nm)/MBT/Au(100). (b) Calculated spectrum of (a), where the Bose-Einstein thermal factor [BE] and the scattering efficiency factor [Scat] are reduced, and EF_{ESERS} spectrum obtained from the background profile of $I_{\text{ESERS}}/I_{\text{ERS}}$. (c) χ''_{SERS} spectrum of (a) and χ''_{RS} spectrum for MBT/Au(100).

3. SERS spectra on roughened metal surfaces

Figure S5 shows the measured ERS and the calculated χ''_{ERS} spectra for a flat polycrystalline Au and also the measured ESERS and the calculated χ''_{ESERS} spectra for a roughened polycrystalline Au. The cross section of ERS is small in the low Raman-shift region because light-induced charge fluctuations are largely screened by Coulomb interaction. The appearance for polycrystalline Au is a kind of averaged spectrum between Au(111) and Au(100). In the ESERS spectrum, the signal intensity is unexpectedly large in the low Raman-shift region probably due to the momentum transfer from microscopic surface roughness.

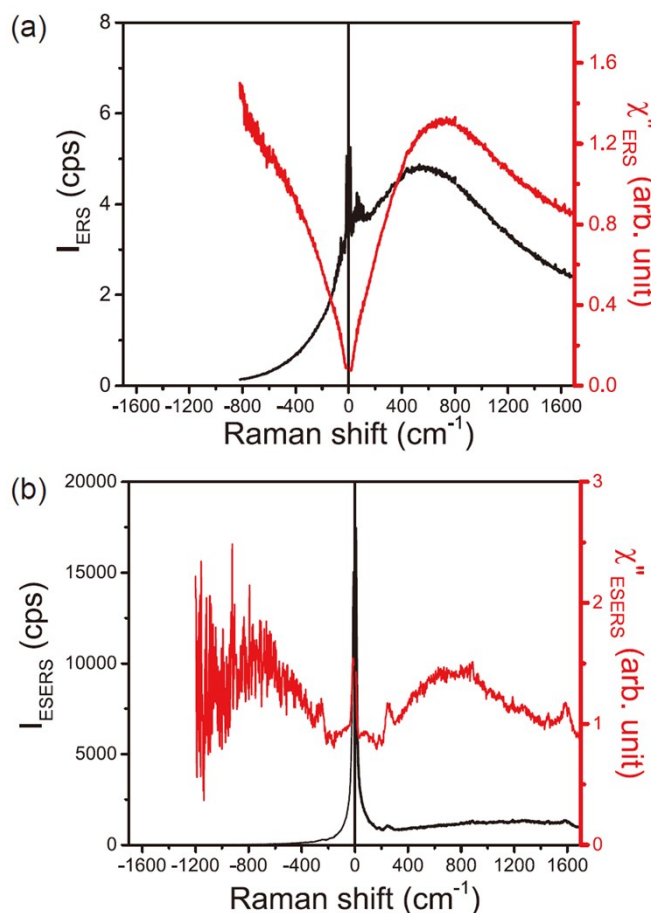


Figure S5. (a) The measured and calculated spectra for ERS at flat polycrystalline Au. (b)

The measured and calculated spectra for ESERS at roughened polycrystalline Au.

4. Estimation of local temperatures

In this study, all of the normal Raman and the SERS spectra were analyzed by assuming the local temperature of 300 K, except for Fig. 8(a). Since the high power excitation may heat up the sample surface, the dependence of ESERS spectra for rough Au on laser pump power, shown in Fig. 8(a), was analyzed by considering the increase of the local temperature. Figure S6 shows an example of the local temperature estimation. When SERS spectrum for rough Au, under the illumination of 11.65 mW, is converted to the χ''_{ESERS} spectrum by using the local temperature of 300 K, the calculation result becomes quite asymmetric for the Stokes and the anti-Stokes branches, as shown in the black curve in Fig. S6. The deviation from the symmetric appearance between these branches can be minimized by adjusting the local temperature value in Eqs. (8) and (9). This procedure enables us to estimate the local temperature.

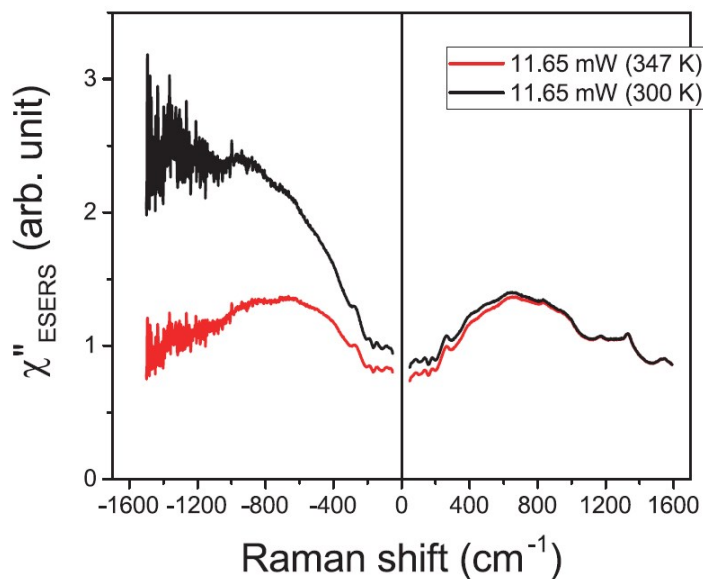


Figure S6. χ''_{ESERS} spectra for rough Au under the illumination of 11.65 mW corrected for local temperatures of 300 and 347 K.

Figure S7 shows the local temperatures of the rough Au surface as a function of laser pump power. The corresponding χ''_{ESERS} spectra under excitation of more than 0.12 mW are shown in Fig. 8. When the pump power was less than 0.12 mW, the measured spectra were able to be analyzed using the local temperature of 300 K. The obtained pump power dependence of the local temperature was well fitted with the power function with the exponent of 0.85.

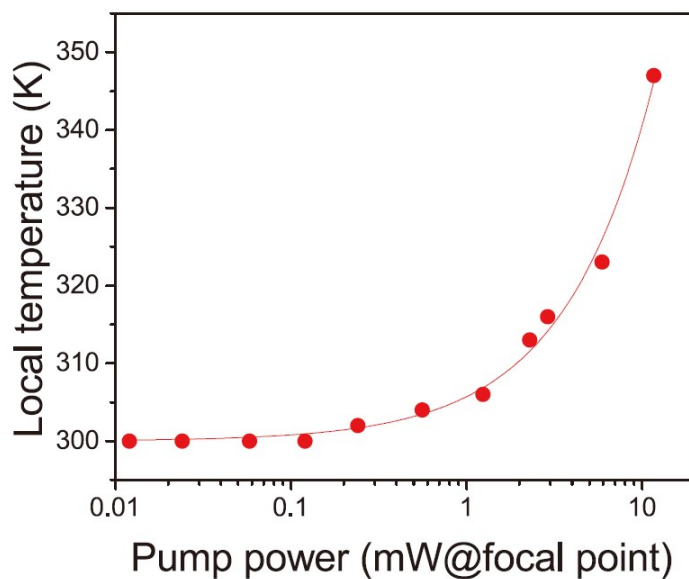


Figure S7. Pump power dependence of local temperatures for the rough Au surface during SERS measurements.